# Photovoltaic Effects of CdS and PbS Quantum Dots Encapsulated in Zeolite Y

**ARTICLE** *in* LANGMUIR · DECEMBER 2011

Impact Factor: 4.46 · DOI: 10.1021/la2025395 · Source: PubMed



**3 AUTHORS**, INCLUDING:

Hyun Sung Kim
Pukyong National University
**884** PUBLICATIONS **15,575** CITATIONS
SEE PROFILE

Nak Cheon Jeong
Daegu Gyeongbuk Institute of Science and T…
**36** PUBLICATIONS **1,289** CITATIONS
SEE PROFILE

Langmuir

ARTICLE

pubs.acs.org/Langmuir

# Photovoltaic Effects of CdS and PbS Quantum Dots Encapsulated in Zeolite Y

Hyun Sung Kim,[§] Nak Cheon Jeong,[§] and Kyung Byung Yoon*

Korea Center for Artificial Photosynthesis, Center for Nano Materials, Department of Chemistry, Sogang University, Seoul 121-742, Korea

Supporting Information

**ABSTRACT:** Zeolite Y films (0.35−2.5 $\mu$m), into which CdS and PbS quantum dots (QDs) were loaded, were grown on ITO glass. The CdS QD-loaded zeolite Y films showed a photovoltaic effect in the electrolyte solution consisting of $Na_2S$ (1 M) and NaOH (0.1 M) with Pt-coated F-doped tin oxide glass as the counter electrode. In contrast, the PbS QD-loaded zeolite Y films exhibited a negligible PV effect. This contrasting behavior was proposed to arise from the large difference in driving force for the electron transfer from $S^{2-}$ in the solution to the hole in the valence band of QDs, with the former being much larger (~2 eV) than the latter (~1 eV). In the case of CdS QD-loaded zeolite Y with a loaded amount of CdS of 6.3 per unit cell, the short circuit current, open circuit voltage, fill factor, and efficiency were 0.3 mA $cm^{-2}$, 423 V, 28, and 0.1%, respectively, under the AM 1.5, 100 mW $cm^{-2}$ condition. This cell was stable for more than 18 days of continuous measurements. A large (3-fold) increase in overall efficiency was observed when PbS QD-loaded zeolite Y on ITO glass was used as the counter electrode. This phenomenon suggests that the uphill electron transfer from ITO glass to S in the solution is facilitated by the photoassisted pumping of the potential energy of the electron in ITO glass to the level that is higher than the reduction potential of S by PbS QDs. Under this condition, the incident-photon-to-current conversion efficiency (IPCE) value at 398 nm was 42% and the absorbed-photon-to-current conversion efficiency (APCE) value at 405 nm was 82%. The electrolyte-mediated interdot charge transport within zeolite films is concluded to be responsible for the overall current flow.

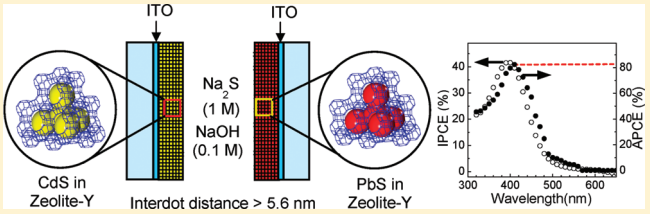


## INTRODUCTION

The development of third-generation photovoltaic devices based on semiconductor quantum dots (QD) is currently receiving a great deal of attention. Among various types of QD-based photovoltaic devices,[1−19] the photovoltaic devices based on 3D QD arrays[1] have received the most attention stemming from the theoretical prediction that its overall conversion efficiency can reach over 44%, although significant challenges with regard to carrier transport within the system are necessary to reach this theoretical limit. As a test case, photovoltaic devices based on PbS and PbSe QD arrays, respectively, have been successfully demonstrated.[1−7]

Zeolite is a class of aluminosilicate minerals having void spaces often called cages or channels.[20] Its general formulation is $M_x[(AlO_2)_x(SiO_2)_y]\cdot nH_2O$. Because each aluminum atom leads to the presence of a negative charge, charge-compensating cations ($M^+$) must be introduced into the structure. The cages or channels are normally filled with cations and water. These cations can be readily substituted with a variety of other cations via conventional aqueous ion exchange. The cavity-filling water molecules are readily lost and regained reversibly without damaging the framework structure. When dehydrated, other guest molecules can occupy the void spaces as long as the interior spaces are large enough and the aperture sizes allow passage of the substrates. Typically, the aperture size of zeolite pores ranges from 0.3 to 0.8 nm, and the inner diameter of interior spaces ranges from 0.5 to 1.3 nm. The structure of zeolite Y is shown in Figure 1a; its aperture size is 0.74 nm, and the diameter of the supercage is 1.3 nm.

Zeolites have been widely tested as hosts for semiconductor QDs.[21−37] Among various types of zeolites, zeolite Y has been the most extensively studied as the host for the generation of very small (<1.5 nm) QDs, organizing them into regular arrays, and stabilizing them for extended periods of time.[21−33] The QDs include various metal chalcogenide (MCh) QDs such as CdS, CdSe, PbS, PbSe, and others.[21−33] They are usually prepared according to eq 1

$$\mathrm{dry}[M^{2+}]_Y + \mathrm{dry}H_2Ch \rightarrow \mathrm{dry}[2H^+, MCh]_Y \quad (1)$$

where $[\ ]_Y$ represents the supercage of zeolite Y and $H_2Ch$ represents hydrogen chalcogenides such as $H_2S$, $H_2Se$, and $H_2Te$.[30−33] In fact, for a given zeolite Y with the unit cell formula $Na_{59}[(AlO_2)_{59}(SiO_2)_{33}]\cdot nH_2O$, the intrazeolite local pH becomes 0.96 when 1 out of 59 $Na^+$ ions is replaced by a $H^+$ ion and becomes −0.4 when 23 out of 59 $Na^+$ ions are replaced by 23 $H^+$

**Received:** July 5, 2011
**Revised:** October 13, 2011
**Published:** October 13, 2011

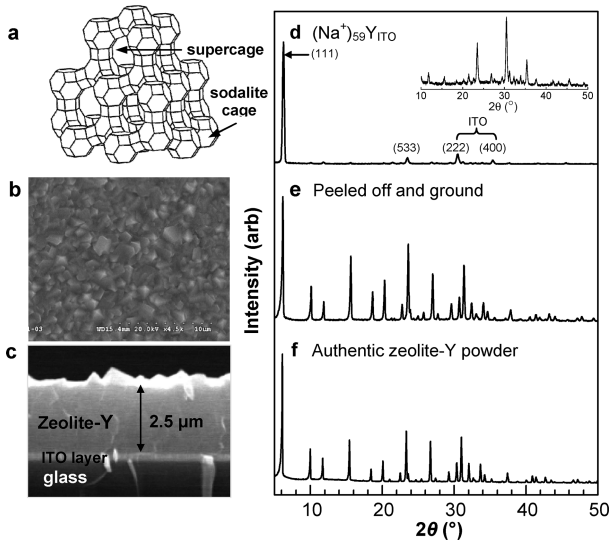


**Figure 1.** Structure of zeolite Y (a), SEM image of a zeolite Y film grown on ITO glass (b, top view; c, side view), X-ray diffraction patterns of a $(Na^+)_{59}Y_{ITO}$ film (d), the zeolite layer peeled off of the ITO glass and ground (e), and authentic zeolite Y powder (f).

ions (SI-1). Thus, MCh QDs inevitably exist in very strongly acidic media if they are produced in zeolite Y according to eq 1.

The MCh QDs produced in zeolite Y are classified as isolated QDs, interconnected QDs, and mesosized QDs.[30,31] The isolated QDs are very small QDs with sizes of less than 1.3 nm existing within a supercage. When MCh QDs are produced in zeolite Y according to eq 1, only isolated QDs are formed. Under some conditions, MCh QDs are also formed in sodalite cages.[28,29] The isolated QDs undergo interconnection at the windows upon adsorption of small amounts of water or methanol. These QD clusters are called interconnected QDs. However, when larger amounts of moisture are introduced into dry MCh-incorporating powder or when dry MCh-incorporating powder is exposed to the atmosphere, the crystalline zeolite Y framework rapidly decomposes into amorphous aluminosilicate particles. Simultaneously, the isolated QDs residing in supercages rapidly aggregate into mesosized QDs that are 3−10 nm in size. The mesosized QDs exist within mesosized internal voids formed within the amorphous aluminosilicate particles and on their external surfaces. However, coating the surface of dry MCh-incorporating powder with octadecyltrichlorosilane (ODC) effectively preserves both the zeolite Y structure and isolated QDs by preventing moisture adsorption into MCh-incorporating powder even in the atmosphere.[30] Alternatively, the neutralization of $H^+$ in dry $[2H^+, MCh]_Y$ to dry $[2NH_4^+, MCh]_Y$ by introducing dry $NH_3$ gas into dry $[2H^+, MCh]_Y$ also leads to the effective preservation of isolated QDs within zeolite Y even in the atmosphere.[33] Thus, under a neutral or basic environment, the isolated QDs in zeolite Y powder are stable even in a moist environment. The absorption maxima ($\lambda_{max}$ values) of isolated, interconnected, and mesosized QDs appear at <295, 300−400, and >400 nm, respectively, in the case of CdS[30,32] and at <295, 300−400, and >400 nm, respectively, in the case of PbS.[31]

Knowing that 3D QD arrays can form third-generation photovoltaic cells,[1−7] we find that it is of great interest to study the photovoltaic effects of the intrazeolite MCh QDs in zeolite Y and their characteristics. We now report that the interconnected CdS QDs show a photovoltaic effect with an absorbed photon-to-current conversion efficiency (APCE) of 81% at 410 nm.

## EXPERIMENTAL SECTION

**Materials.** Sodium silicate ($Na_2SiO_3$, 17−19% $Na_2O$ and 35−38% $SiO_2$, Kanto), sodium aluminate ($NaAlO_2$, $Na_2O$ = 31−35%, and $Al_2O_3$ = 34−39%, Kanto), sodium hydroxide (NaOH, Samchun), cadmium nitrate tetrahydrate ($Cd(NO_3)_2 \cdot 4H_2O$, Junsei), lead nitrate tetrahydrate ($Pb(NO_3)_2$, Junsei), hydrogen sulfide ($H_2S$, Regas), and sodium sulfide nonahydrate ($Na_2S \cdot 9H_2O$, Aldrich) were used as received. Zeolite Y (lot no. 1997060001) with an average particle size of ~1.5 $\mu$m was purchased from UOP. Indium tin oxide (ITO) glass (400 × 370 $mm^2$, 7.5 Ω $cm^{-1}$, Samsung-Corning) was cut into smaller pieces (25 × 30 $mm^2$). F-doped tin oxide glass (FTO glass, 8 Ω $cm^{-1}$, thickness of the FTO layer = 100 nm, thickness of glass support = 3 mm) was purchased from Libby Owens Ford. Thermoplastic film (Surlyn) with a thickness of 100 $\mu$m was a product of DuPont. Mucasol (Merz Co.) was purchased and used as received.

**Preparation of $(Na^+)_{59}Y$ Films Supported on ITO Glass ($(Na^+)_{59}Y_{ITO}$).** Zeolite Y seed crystals (80 nm, 1 g) were dispersed in distilled deionized water (1 L). Independently, several pieces of ITO glass (25 × 30 $mm^2$) were washed by sonicating the ITO glass plates in a Mucasol solution (3%) for 10 min and subsequently washed with copious amounts of water. The aqueous suspension of the seed crystals was spin coated twice onto the ITO side at a speed of 2000 rpm. The seeded glass plates were then kept for 30 min in an oven preheated to 100 °C. After being cooled to room temperature, the seeded glass plates were placed vertically on a Teflon support. The support was then immersed in a synthesis gel with a molar composition of 14:1:10:720 $Na_2O/Al_2O_3/SiO_2/H_2O$, and the reactor was placed for 12 h in an oven preheated to 100 °C. The average thickness of the resulting zeolite Y films was 2.5 $\mu$m. The Si/Al ratio of the zeolite Y film was 1.8, indicating that the composition of zeolite Y is $M_{59}[(AlO_2)_{59}(SiO_2)_{33}] \cdot nH_2O$. On the basis of this formula, we denote the zeolite film as $(Na^+)_{59}Y_{ITO}$.

**Preparation of $(CdS)_n$- and $(PbS)_n$-Containing Zeolite Y Films Supported on ITO Glass ($(CdS)_nY_{ITO}$ and $(PbS)_nY_{ITO}$).** A $(Na^+)_{59}Y_{ITO}$ film was immersed into each 25 mL aliquot of $Cd(NO_3)_2$ and $Pb(NO_3)_2$ solutions of different concentrations ($x$ = 0.01, 0.05, and 0.1 mM) for 10 min at room temperature. The $Cd^{2+}$- or $Pb^{2+}$-exchanged $Y_f$ films supported on ITO glass were washed with copious amounts of distilled deionized water, and subsequently dried under a stream of $N_2$. The amounts of ion exchange were 3.2, 4.3, and 6.3 for $Cd^{2+}$ and 3.4, 4.6, and 6.7, respectively for $Pb^{2+}$, per unit cell. They are denoted as $(Cd^{2+})_nY_{ITO}$ ($n$ = 3.2, 4.3, and 6.3) and $(Pb^{2+})_nY_{ITO}$ ($n$ = 3.4, 4.6, and 6.7). The $(Cd^{2+})_nY_{ITO}$ and $(Pb^{2+})_nY_{ITO}$ films were introduced into a Schlenk tube and dried at 200 °C for 12 h under vacuum (<$10^{-5}$ Torr). After being cooled to room temperature, dry $H_2S$ gas was introduced into the Schlenk tube and the tube was kept for 30 min at room temperature to generate CdS and PbS QDs in zeolite Y. The remaining unreacted $H_2S$ gas was pumped off of the tube. The obtained $(CdS)_n$- and $(PbS)_n$-containing zeolite Y films are denoted as $(CdS)_nY_{ITO}$ and $(PbS)_nY_{ITO}$, respectively, where $n$ = 3.2, 4.3, and 6.3 for the case of CdS per unit cell and 3.4, 4.6, and 6.7 for the case of CdS per unit cell.

**Analyses of the Loaded Amounts of CdS and PbS in Zeolite Y Films.** The Si/Al ratio of the zeolite Y films and the number of $Cd^{2+}$ and $Pb^{2+}$ ions in zeolite Y films were analyzed from the energy-dispersive X-ray (EDX) spectra of the samples using a Horiba EMAX 6853-H EDX spectrometer. To obtain reliable data, the elements to be analyzed were limited to two at a time. For example, Si and Al were selected at the time of elemental analysis by EDX. The Si/Al ratios of the zeolites were determined in this way. After the Si/Al ratio was determined, elemental analyses were carried out for Al and Na, Al and Cd, Al and Pb, and Al and S. After obtaining these series of ratios for Al/Si, Al/Na, Al/Cd, Al/Pb, and Al/S, we assigned the unit cell formula based

**Table 1. Compositions of CdS- and PbS-Loaded Zeolite Y Films Used in This Study**

| type | composition |
|---|---|
| $(CdS)_{3.2}Y_{ITO}$ | $Cd_{3.2}S_{3.1}H_{6.2}Na_{63.6}Al_{70}Si_{122}O_{384}$ |
| $(CdS)_{4.3}Y_{ITO}$ | $Cd_{4.3}S_{4.2}H_{8.4}Na_{61.4}Al_{70}Si_{122}O_{384}$ |
| $(CdS)_{6.3}Y_{ITO}$ | $Cd_{6.3}S_{6.1}H_{12.2}Na_{57.4}Al_{70}Si_{122}O_{384}$ |
| $(PbS)_{3.4}Y_{ITO}$ | $Pb_{3.4}S_{3.2}H_{6.4}Na_{63.2}Al_{70}Si_{122}O_{384}$ |
| $(PbS)_{4.6}Y_{ITO}$ | $Pb_{4.6}S_{4.4}H_{8.8}Na_{60.8}Al_{70}Si_{122}O_{384}$ |
| $(PbS)_{6.7}Y_{ITO}$ | $Pb_{6.7}S_{6.5}H_{13.0}Na_{56.6}Al_{70}Si_{122}O_{384}$ |

on the unit cell structure of zeolite Y. The results are shown in Table 1. This procedure gives quite reliable data for the elemental analyses for these elements. One important point during this procedure is not to include the oxygen atom as the element to be analyzed because it is a relatively light element and its amount is variable depending on the pretreatment of zeolites.

**Preparation of ODC-Coated $(CdS)_nY_{ITO}$ and $(PbS)_nY_{ITO}$ (ODC-$(CdS)_nY_{ITO}$ and ODC-$(PbS)_nY_{ITO}$).** Dry $(CdS)_nY_{ITO}$ and $(PbS)_nY_{ITO}$ were transferred to a drybox charged with high-purity argon. One piece of $(CdS)_nY_{ITO}$ or $(PbS)_nY_{ITO}$ was placed with the zeolite Y film side facing upward into the glass vial (diameter = 4 cm) containing 4 mL of octadecyltrichlorosilane as a surface-silylating agent (neat). The surface-silylating agent was heated to 90 °C for 30 min by placing the glass vial on top of a temperature-controlled hot plate. After 30 min, the reaction mixture was cooled to room temperature and then washed with copious amounts of dry *n*-hexane several times. After being washed, ODC-coated $(CdS)_nY_{ITO}$ was dried by evacuation for 20 min in the drybox.

**Preparation of Two-Holed Pt-Coated FTO Glass Plates (2h-$Pt_{FTO}$).** Several FTO glass plates were prepared, and on each FTO glass plate ($20 \times 20$ mm$^2$), two holes with a diameter of 0.75 mm were made from the FTO side to the glass side using a small diamond-coated drill tip with a diameter of 0.75 mm at positions (−3.0 mm, −3.0 mm) and (3.0 mm, 3.0 mm) from the center of the plate, where the horizontal and vertical edges are defined as the *x* and *y* axes, respectively (SI-2). The FTO glass plates with two holes were coated with Pt by rf sputtering. The two-holed Pt-coated FTO glass is denoted as 2 h-$Pt_{/FTO}$.

**Fabrication of PV Cells.** A Surlyn tape spacer ($20 \times 20$ mm$^2$, thickness = 100 $\mu$m) having a square hole of $10 \times 10$ mm$^2$ size was sandwiched between $(MCh)_nY_{ITO}$ and 2 h-$Pt_{/FTO}$. The sandwiched assembly was placed on a hot plate whose temperature was maintained at 130 °C and pressed for 7 min under a pressure of 1.2 N·m. After being cooled to room temperature, the electrolyte solution was introduced into the void space created between the two electrodes through one of the holes. The electrolyte solution was composed of 0.1 M $Na_2S$ and 1 M NaOH. After filling up the void space with the electrolyte solution, the holes were blocked with small glass plates using Surlyn as the adhesive.

**Photocurrent Measurements.** Photocurrent measurements were conducted under a standard condition of 1 sun (100 mW·cm$^{-2}$, AM 1.5 filter). The IPCE and APCE spectra were determined from eqs 2 and 3, respectively,

$$\mathrm{IPCE}(\%) = \frac{1240}{\lambda} \times \frac{J_{sc}}{I_{in}} \times 100 \quad (2)$$

$$\mathrm{APCE}(\%) = \frac{\mathrm{IPCE}}{1 - T} \quad (3)$$

where $\lambda$ is the excitation wavelength, $J_{sc}$ is the short circuit photocurrent (A·cm$^{-2}$), $I_{in}$ is the incident light intensity (W·cm$^{-2}$), and $T$ is the transmittance expressed as $10 \times 10^{-A}$, where $A$ is the absorbance.

**Instrumentation.** The $\theta-2\theta$ scans of Y films were performed on a Rigaku Ultima 4 with a power of 40 kV and 40 mA. The wavelength of the monochromated X-ray beam was 1.5406 nm generated from Cu K$\alpha$ radiation. Diffuse-reflectance UV−vis spectra of the samples were recorded on a Varian Cary 5000 UV−vis−NIR spectrophotometer equipped with an integrating sphere. Barium sulfate ($BaSO_4$) was used as the reference. The diffuse reflectance spectra were converted into the Kubelka−Munk (K−M) formalism. To obtain the transmittance spectra of CdS QDs in the zeolite Y film, a $(CdS)_nY_{ITO}$ plate with a size of $9 \times 40$ mm$^2$ was placed in a rectangular quartz UV−vis cell ($10 \times 10 \times 40$ mm$^3$) and DMSO was used to fill the UV cell as an index-matching fluid. A UV−vis cell filled with DMSO was used as the reference cell. For comparison and to extract the transmittance spectra of only CdS QDs in $(CdS)_nY_{ITO}$, the transmittance spectrum of $(Na)_{59}Y_{ITO}$ was also obtained. For this, a $(Na)_{59}Y_{ITO}$ plate with the size of $9 \times 40$ mm$^2$ was placed in the quartz UV−vis cell filled with DMSO. Scanning electron microscopy (SEM) images of the films were obtained using a field-emission scanning electron microscope (Hitachi S-4300) operating at an acceleration voltage of 20 kV. The Si/Al ratio of the zeolite Y films, and the number of $Cd^{2+}$ and $Pb^{2+}$ ions in zeolite Y films were analyzed from the energy-dispersive X-ray (EDX) spectra of the samples using a Horiba EMAX 6853-H EDX spectrometer. AFM images were obtained from a JEOL scanning probe microscope (JSPM-5410). Current−voltage ($J-V$) curves were obtained from a Keithley 2400 source meter under the light produced from an Oriel 191 solar simulator equipped with an AM 1.5 filter. The light source was an Oriel 1000 W Xe lamp. The applied light intensity was 100 mW cm$^{-2}$. The intensity of the incident light was calibrated using a KG5-filtered, monocrystalline Si reference solar cell, PVM 37 (ISO tracking number 1006), which was calibrated at the National Renewable Energy Laboratory in Golden, Colorado. Each data point in the tables represents the average value obtained from three samples. The IPCE spectra for the cells were measured on an IPCE measuring system (PV Measurements) in which monochromatic light is generated using a tungsten light source filtered by a grating monochromator and order-sorting filters. The light was modulated with a mechanical chopper (Digirad C-980). A broad band light was simultaneously applied to the sample cell to bring the cell under end-use conditions. The current generated by the sample cell at a specific voltage is converted to a voltage by a transimpedance amplifier and measured with a lock-in amplifier (Stanford Research Systems SR810) synchronized to the mechanical chopper. The photon flux of the monochromatic light was determined by measuring the signal produced by a calibrated photodiode and comparing the signal to the photodiode's known spectral response information.

## RESULTS AND DISCUSSION

**Characterization of $(Na^+)_{59}Y_{ITO}$.** The zeolite Y films were strongly adhered to ITO glass plates because of the strong binding of the zeolite Y film to the ITO glass.[30,31] The typical scanning electron microscope (SEM) image of a $(Na^+)_{59}Y_{ITO}$ plate (top view) is shown in Figure 1b. The typical thickness was 2.5 $\mu$m as the cross-sectional SEM image (Figure 1c) shows. The X-ray diffraction pattern of the zeolite film shown in Figure 1d looks different from the typical diffraction pattern of zeolite Y powder. The intense peak at $2\theta = 6.20°$ arises from the diffraction by the zeolite Y (111) plane, and the weak peak at 23.59° arises from the diffraction by the zeolite Y (533) plane. The two diffraction peaks at $2\theta = 30.58°$ and 35.72° arise from the diffractions by the (222) and (400) planes of the ITO substrate, respectively. To be sure about the structure of the zeolite film, we peeled the zeolite layer off of the ITO glass, and the zeolite fragments that were removed were further ground into a fine powder. The X-ray powder diffraction pattern of the fine powder (Figure 1e) matched very well with that of an

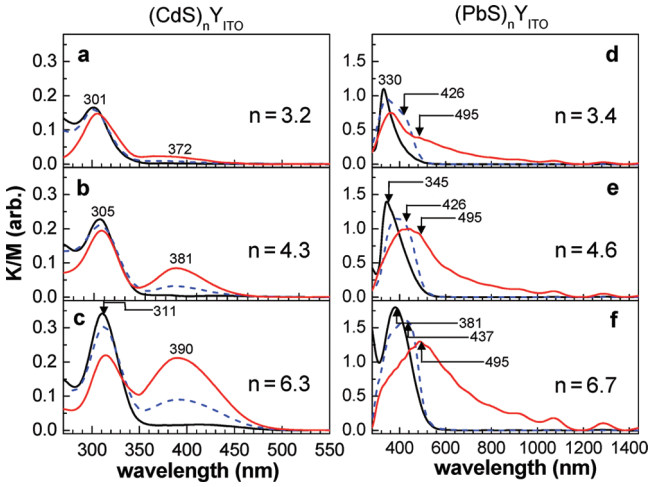


**Figure 2.** Diffuse-reflectance UV−vis spectra of $(CdS)_{3.2}Y_{ITO}$ (a), $(CdS)_{4.3}Y_{ITO}$ (b), $(CdS)_{6.3}Y_{ITO}$ (c), $(PbS)_{3.4}Y_{ITO}$ (d), $(PbS)_{4.6}Y_{ITO}$ (e), and $(PbS)_{6.7}Y_{ITO}$ (f) after three different types of treatment: ODC coating (black solid line) after exposure to the atmosphere for 24 h (blue dashed line) and after immersion in the electrolyte solution for 12 h (red solid line), respectively.

authentic zeolite Y powder (Figure 1f). This confirms that the zeolite film grown on ITO glass is indeed zeolite Y. We also found that other zeolites such as zeolite A, zeolite X, and ETS-10 grow equally well on ITO and FTO glass plates (SI-3). In contrast, none of the above zeolites grew satisfactorily on ordinary glass plates, owing to the dissolution of the surfaces of glass plates by strongly basic gels (SI-3). This indicates that the ITO and FTO layers serve not only as the strong adhesion layers for zeolite films but also as the surface-protecting layers effectively protecting the glass surfaces from corrosion by strong basic media.

By taking the fact that there are eight supercages per unit cell into account, the incorporated amounts of CdS in $(CdS)_nY_{ITO}$ ($n$ = 3.2, 4.3, and 6.3) correspond to 0.40, 0.54, and 0.79 CdS per supercage and the incorporated amounts of PbS in $(PbS)_nY_{ITO}$ (3.4, 4.6, and 6.7) correspond to 0.43, 0.58, and 0.84 PbS per supercage, respectively. Thus, the incorporated amounts are in fact very small when compared to the volume of a supercage (1150 Å$^3$), which, on the basis of a theoretical consideration, can accommodate up to 1.3-nm-sized CdS nanocrystals composed of 23 CdS units. The incorporated amounts are also small (3.2−6.7 puc or 11−22%) even from the point of view of the maximum capacity (30 puc) calculated from the ion exchange capacity. Therefore, we attempted to increase the loaded amounts. Unfortunately, however, the CdS- and PbS-loaded zeolite Y films underwent crack formation upon increasing the loaded amounts. In any case, another point to note is that the incorporated amounts of CdS and PbS are nearly the same in $(CdS)_nY_{ITO}$ and $(PdS)_nY_{ITO}$ ($n$ = 3.2 vs 3.4, 4.3 vs 4.6, and 6.3 vs 6.7).

**Analysis of the UV−Vis Spectra of $(CdS)_nY_{ITO}$ and $(PbS)_nY_{ITO}$ in the Dry State.** The diffuse-reflectance UV−vis spectra of $(CdS)_nY_{ITO}$ and $(PbS)_nY_{ITO}$ after three different postsynthetic treatments (vide infra) are shown in Figure 2a−f for each loading level. As noted from the difference in the intensity scales between the left and right, extinction coefficients for the intrazeolite PbS QDs are about 5 times higher than those of intrazeolite CdS QDs.

The black-solid spectra show the spectra of ODC-coated dehydrated $(CdS)_nY_{ITO}$ and $(PbS)_nY_{ITO}$ plates (denoted as ODC-$(CdS)_nY_{ITO}$ and ODC-$(PbS)_nY_{ITO}$, respectively). They can be regarded as the spectra of isolated CdS and PbS QDs (vide supra) as reported earlier.[31,32] The fact that ODC-$(CdS)_nY_{ITO}$ and ODC-$(PbS)_nY_{ITO}$ do not absorb wavelengths longer than 350 and 580 nm, respectively, confirms that only isolated QDs are formed during their formation in the dry state. The progressive red shift of the absorption maximum ($\lambda_{max}$) of the isolated CdS QDs (from 300 to 311 nm) and the increase in intensity upon increasing the loaded amount (from 3.2 to 6.3 puc) indicate that the average size and number of isolated CdS QDs increase simultaneously. The $\lambda_{max}$ values of the isolated QDs in ODC-$(CdS)_nY_{ITO}$ are red shifted by up to 20 nm compared to those previously observed from zeolite powders (295 nm). From this phenomenon, we newly deduced the following three behaviors of zeolites. First, the isolated QDs tend to grow as large as possible in zeolite pores to increase their stabilities. Second, the sizes of the isolated QDs that have been produced in zeolite Y powders in the earlier reports have not yet reached their maximum size. Third, the probability of the isolated QDs growing larger increases with increasing the volume of the host for a given loading level, that is, upon shifting the host from individual powders with an average volume of $3 \times 3 \times 3\ \mu m^3$ to continuous films with a volume of $2.5 \times 20\,000 \times 20\,000\ \mu m^3$.

Similar phenomena were observed for $(PbS)_nY_{ITO}$ (Figure 2d−f). Thus, isolated PbS QDs appeared in the 330−380 nm region and $\lambda_{max}$ progressively red shifted from 330 to 345 and to 381 nm with increasing $n$ from 3.4 to 4.6 and to 6.7 (black spectra). Calzaferri and co-workers assigned the absorption band with $\lambda_{max}$ < 380 nm as the absorption of the PbS monomer residing in zeolite A.[35] We also assign the 330 nm band of PbS encapsulated in zeolite Y as the monomer PbS band.

**Analysis of the UV−Vis Spectra of $(CdS)_nY_{ITO}$ and $(PbS)_nY_{ITO}$ after Exposure to the Atmosphere.** Upon exposure of a $(CdS)_nY_{ITO}$ plate to the atmosphere, the absorption intensity of isolated QDs slightly decreased and the absorption band due to interconnected QDs appeared in the 350−400 nm region (Figure 2a−c, blue dashed spectra). The $\lambda_{max}$ values of the interconnected CdS QDs in the zeolite Y film (372−390 nm) also substantially red shifted with respect to those observed from the individual zeolite Y microcrystals (300−370 nm). It is also interesting that the $\lambda_{max}$ value of the interconnected QDs in $(CdS)_nY_{ITO}$ progressively red-shifted (from 372 to 390 nm) upon increasing the CdS loading. This phenomenon is attributed to the increase in the total amount of CdS in a closed system upon increasing the size of the zeolite host from individual 1 to 2 $\mu$m-scale small crystals to the centimeter-scale film. The progressive increase in the interconnected CdS band in $(CdS)_nY_{ITO}$ with increasing $n$ also indicates that the amount of interconnected CdS increases as $n$ increases.

Likewise, the exposure of $(PbS)_nY_{ITO}$ to the atmosphere slowly (over a period of 12 h) induced the formation of interconnected PbS QDs with their $\lambda_{max}$ values appearing in the 420−470 nm region and progressively red shifting with increasing $n$ (blue dashed spectra in Figure 2d−f). The progressive increase in the interconnected PbS band also indicates that the amount of interconnected PbS increases as $n$ increases.

In fact, when zeolite Y exists in the powder form, dry $[2H^+, CdS]_Y$ and $[2H^+, PbS]_Y$ rapidly undergo framework decomposition and the formation of mesosized QDs on the surface upon exposure to the atmosphere.[31,32] The aforementioned strongly


dx.doi.org/10.1021/la2025395 |Langmuir 2011, 27, 14678–14688

acidic medium of $[2H^+, CdS]_Y$ in the moist environment (vide supra) has been regarded to be responsible for the framework rupture. In view of this, the behaviors of the corresponding films, namely, $(CdS)_nY_{ITO}$ and $(PbS)_{6.7}Y_{ITO}$ (no framework destruction but instead the formation of interconnected QDs), were quite surprising to us despite the fact that they are generated according to eq 1. The reason is not yet clear at this stage. The 1D adsorption of water into the zeolite film might be one of the important reasons for the occurrence of this interesting phenomenon.

Knowing that $NH_3$-treated $[2H^+, CdS]_Y$, namely, $[2NH_4^+, CdS]_Y$, does not form either interconnected CdS QDs within the framework nor mesosized CdS QDs with accompanying framework decomposition even after exposure to the moist atmosphere,[33] we also treated dry $(CdS)_{6.3}Y_{ITO}$ (can also be denoted as $(2H^+, CdS)_{6.3}Y_{ITO}$]) with $NH_3$ and then exposed the dry $NH_3$-treated $(CdS)_{6.3}Y_{ITO}$ (can also be denoted as $(2NH_4^+, CdS)_{6.3}Y_{ITO}$) to the atmosphere. Like the case of $[2NH_4^+, CdS]_Y$ powder, the diffuse-reflectance UV−vis spectrum of $NH_3$-treated $(CdS)_{6.3}Y_{ITO}$ (or $(2NH_4^+, CdS)_{6.3}Y_{ITO}$) was the same as that of dry $(2H^+, CdS)_{6.3}Y_{ITO}$ even after exposure to the atmosphere for 24 h (SI-4).

**Analysis of the UV−Vis Spectra of $(CdS)_nY_{ITO}$ and $(PbS)_nY_{ITO}$ after Immersion in the Electrolyte Solution.** In the case of $(CdS)_nY_{ITO}$, the band due to the isolated CdS QDs decreased further whereas the band due to the interconnected CdS QDs increased (Figure 2a−c, red solid curves). In the case of $(CdS)_{6.3}Y_{ITO}$, the spectrum shows that the number of interconnected CdS QDs is larger than that of isolated CdS QDs. The spectra did not change even after immersing the films for an extended period of time (1 day).

In the case of $(PbS)_nY_{ITO}$, a shoulder band with $\lambda_{max} = 495$ nm appeared in the cases of $n = 3.4$ and 4.6. This phenomenon was dominant when $n = 6.7$ (red spectra). In the case of $(PbS)_{6.7}Y_{ITO}$, small absorption bands with $\lambda_{max} = 610$, 700, 800, 950, 1070, and 1300 nm also appeared simultaneously. The spectra also did not change even after immersing the films for an extended period of time (1 day). We assign the 495 nm band as the absorption arising from the interconnected PbS QDs produced by the coalition of a larger number of isolated QDs. Absorption peaks with $\lambda_{max} = 610-1300$ nm are attributed to the exciton absorption bands of 3−5 nm PbS QDs that are produced on the surface of $(PbS)_nY_{ITO}$ as will be discussed in more detail in a later part of this article. From the consideration that PbS QDs have very high extinction coefficients, the estimated amounts of mesosized PbS QDs in $(PbS)_nY_{ITO}$ seem to be very small.

**Analysis of the Framework Structures of $(CdS)_nY_{ITO}$ and $(PbS)_nY_{ITO}$ by X-ray Diffraction Patterns after Immersion in the Electrolyte Solution.** The X-ray diffraction patterns of air-exposed $(CdS)_{6.3}Y_{ITO}$ and $(PbS)_{6.7}Y_{ITO}$ were identical to those of ODC-$(CdS)_{6.3}Y_{ITO}$ and ODC-$(PbS)_{6.7}Y_{ITO}$ (data not shown), indicating that the frameworks of $(CdS)_{6.3}Y_{ITO}$ and $(PbS)_{6.7}Y_{ITO}$ remain intact even under the moist atmosphere. The X-ray diffraction patterns of $(CdS)_{6.3}Y_{ITO}$ and $(PbS)_{6.7}Y_{ITO}$ also did not show noticeable changes in intensity (with respect to those of ODC-$(CdS)_{6.3}Y_{ITO}$ and ODC-$(PbS)_{6.7}Y_{ITO}$) even after immersion in the electrolyte solution for 12 h (SI-5), indicating that the frameworks do not undergo structural decomposition. These results indicate that $(CdS)_{6.3}Y_{ITO}$ and $(PbS)_{6.7}Y_{ITO}$ are quite stable even in the electrolyte solution. Their remarkable stability in the basic electrolyte solution can be likened to the neutralization of $H^+$ ions in $[2H^+, MCh]_Y$ with $NH_3$ under the dry condition (vide supra).[33]

**Characterization of $(CdS)_nY_{ITO}$ and $(PbS)_nY_{ITO}$ with Atomic Force Microscopy.** We further investigated the surfaces of $(Na)_{59}Y_{ITO}$, $(CdS)_{6.3}Y_{ITO}$, and $(PbS)_{6.7}Y_{ITO}$ with an atomic force microscope (AFM). After immersion in the electrolyte solution for 12 h, the films were washed with distilled deionized water and dried before the AFM study. The AFM images of $(Na)_{59}Y_{ITO}$ and $(CdS)_{6.3}Y_{ITO}$ at two different magnifications were nearly the same (SI-6), which confirms the stability of the zeolite framework in $(CdS)_nY_{ITO}$ and the nonformation of mesosized CdS QDs on the surface.

The low-magnification AFM image of $(PbS)_{6.7}Y_{ITO}$ further showed that the framework is stable even after immersion in the electrolyte solution for 12 h. The high-magnification AFM image, however, showed the images that can be attributed to the presence of small amounts of 3−5 nm PbS QDs on the surface, consistent with the UV−vis spectra (Figure 2f). However, this structural damage seems to be occurring only on the outermost few layers of zeolite Y films because X-ray diffraction analyses show that most of the diffraction intensities remain intact even after immersion in the electrolyte solution. The structural damage occurring on the outermost few layers would not affect the overall photovoltaic performances of $(CdS)_{6.3}Y_{ITO}|(PbS)_{6.7}Y_{ITO}$. Thus, unlike $[2H^+, PbS]_Y$ in the powder state, $(PbS)_nY_{ITO}$ is stable in the atmosphere and even in the basic electrolyte solution. The same conclusion was also derived from the characterization of $(PbS)_{6.7}Y_{ITO}$ with transmission electron microscopy (SI-7).

**Photovoltaic Effects of $(CdS)_nY_{ITO}$ and $(PbS)_{6.7}Y_{ITO}$.** The schematic illustrations of $(CdS)_nY_{ITO}|Pt_{FTO}$, $(PbS)_{6.7}Y_{ITO}|Pt_{FTO}$, and $(CdS)_{6.3}Y_{ITO}|(PbS)_{6.7}Y_{ITO}$ are shown in Figure 3 together with their current−voltage ($I-V$) curves under the 1 sun condition (AM 1.5, 100 mW·cm$^{-2}$). The details of their photovoltaic performance data under a 1 sun condition are listed in Table 2.

In the case of $(CdS)_nY_{ITO}|Pt_{FTO}$, $(CdS)_nY_{ITO}$ acts as a photoanode, injecting electrons into ITO glass and receiving electrons from $S^{2-}$ in the electrolyte solution. We propose that the photoassisted electron flow occurs according to the scheme shown in Figure 4a. Thus, the irradiation of a CdS QD in zeolite Y leads to electron excitation from the valence band (VB) to the conduction band (CB). The photoexcited electron is injected into ITO glass, which is subsequently transferred to FTO glass through the external circuit. The electron on FTO glass is then transferred to elemental S, which is produced by the oxidation of $S^{2-}$, catalyzed by the Pt nanoparticles coated on FTO glass. In fact, the overall electron flow occurs even in the absence of Pt nanoparticles on FTO glass, although the overall efficiency decreases, indicating that Pt nanoparticles accelerate the electron transfer between FTO glass and S. The assignments of the lower band edge values of CB and upper band edge values of VB will be described in detail in a later part of this article (vide infra).

In the case of $(PbS)_{6.7}Y_{ITO}|Pt_{FTO}$, albeit inefficient, $(PbS)_{6.7}Y_{ITO}$ acts as a photocathode with $Pt_{FTO}$ as the counter electrode. We propose that the corresponding photoassisted electron flow occurs according to the scheme shown in Figure 4b. Thus, the irradiation of a PbS QD in zeolite Y leads to the electron excitation from VB to CB, and the electron residing in PbS CB is transferred to elemental S in the solution, not to ITO glass. $S^{2-}$ then transfers electrons to FTO glass catalyzed by the Pt nanoparticles that coat the FTO surface. The electron residing in FTO glass is transferred through the electrical wire to the ITO glass, although very inefficiently.

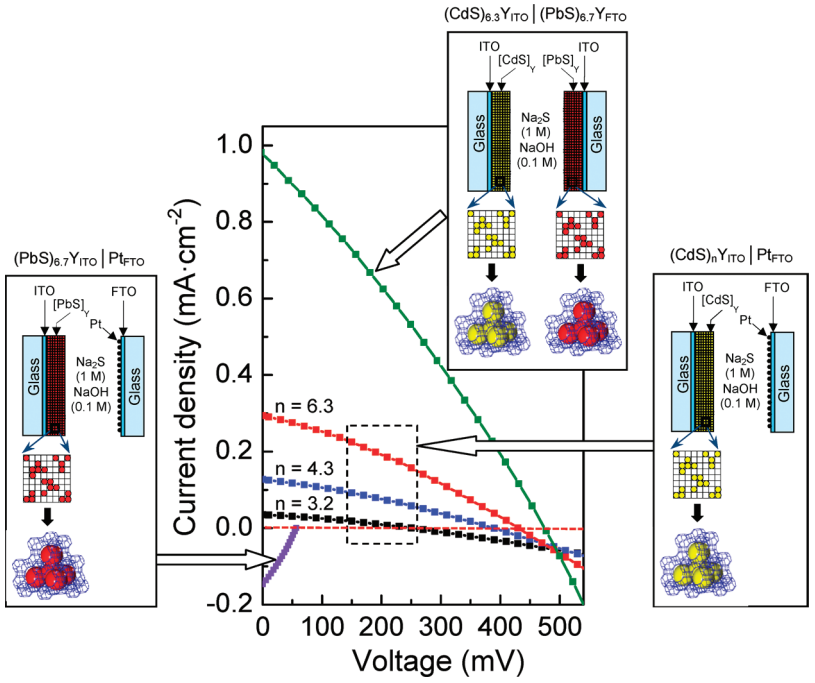


**Figure 3.** Schematic illustrations of the photovoltaic cells used in this study and their $I-V$ curves.

**Table 2. Photovoltaic Characteristics of $(CdS)_nY_{ITO}|Pt_{FTO}$, $(PbS)_{6.7}Y_{ITO}|Pt_{FTO}$ and $(CdS)_{6.3}Y_{ITO}|(PbS)_{6.7}Y_{ITO}$**

| | $I_{sc}$ (mA/cm$^2$)[a] | $V_{oc}$ (mV)[b] | $FF$[c] | $\eta$ (%)[d] |
|---|---|---|---|---|
| $CdS_{3.2}Y_{ITO}|Pt_{FTO}$ | 0.04 | 252 | 27 | ~0.01 |
| $CdS_{4.3}Y_{ITO}|Pt_{FTO}$ | 0.13 | 390 | 30 | 0.04 |
| $CdS_{6.3}Y_{ITO}|Pt_{FTO}$ | 0.30 | 423 | 28 | 0.1 |
| $PbS_{6.7}Y_{ITO}|Pt_{FTO}$ | −0.15 | −58 | 29 | ~0.01 |
| $CdS_{6.3}Y_{ITO}|PbS_{6.7}Y_{ITO}$ | 0.98 | 478 | 30 | 0.30 |

[a] Short circuit current. [b] Open circuit voltage. [c] Fill factor. [d] Efficiency.

The difference between the two QD systems, $(CdS)_nY$ and $(PbS)_{6.7}Y$, is ascribed to the difference in the driving force for the electron transfer from $S^{2-}$ to the hole residing in the VBs of CdS and PbS. Thus, whereas a large energy difference between the two energy levels (1.85−2.05 eV) allows the electron transfer to take place effectively in the case of $(CdS)_nY$, a much smaller energy difference (0.85−1.05 eV) in the case of $(PbS)_{6.7}Y$ makes the electron transfer from $S^{2-}$ to the hole in the VB of PbS take place inefficiently. As a result, whereas the photoexcited electron residing in the CB of CdS is effectively injected into the ITO glass, that of PbS rather recombines with the hole residing in the VB. However, the small cathodic current arising from $(PbS)_{6.7}Y$ indicates that a small portion of the photoexcited electrons are transferred to S in the solution rather than to the ITO glass.

Most interestingly, when $(CdS)_{6.3}Y_{ITO}$ and $(PbS)_{6.8}Y_{ITO}$ were coupled, a 3-fold increase in $\eta$ (from 0.1 to 0.3%) was observed to arise from the marked increases in $I_{sc}$ (from 0.30 to 0.98 mA cm$^{-2}$) and $V_{oc}$ (from 423 to 478 mV) (Table 2). We propose that the photoassisted electron flow occurs according to the scheme shown in Figure 4c. Thus, the irradiation of a CdS QD in zeolite Y leads to the electron excitation from VB to CB. The electron residing in the CB is transferred to the ITO glass. The electron residing in ITO glass is subsequently transferred to FTO glass through the external circuit. The electron in FTO glass is transferred to the hole in VB of a PbS QD created by the photoexcitation of an electron in VB to CB of the PbS QD. The photoexcited electron, now residing in CB, is transferred to S, and the produced $S^{2-}$ transfers electrons to VB of the CdS QD.

Interestingly, in the case of $(CdS)_nY_{ITO}|Pt_{FTO}$, the incident-photon-to-current efficiency (IPCEs) spectrum (Figure 5a) and APCE spectrum (Figure 5b) coincided very well with the corresponding absorption (Kubelka−Munk) spectra of the interconnected QDs but not with those of isolated QDs in all three cases. To obtain the APCE spectra of $(CdS)_nY_{ITO}|Pt_{FTO}$, we independently measured the transmittance spectra of $(CdS)_nY_{ITO}$ and $(Na)_{59}Y_{ITO}$ (SI-8) to obtain the absorbance by only $(CdS)_n$ in each $(CdS)_nY_{ITO}$ film. The above IPCE and APCE data revealed that only the interconnected CdS QDs, but not isolated QDs, are responsible for the photovoltaic effects. The IPCE/APCE values of $(CdS)_nY_{ITO}|Pt_{FTO}$ (in %) at the maximum IPCE (or APCE) wavelength were 4.2/8.5 at 370 nm, 7.4/14.7 at 380 nm, and 15.2/31.3 at 390 nm for $n$ = 3.2, 4.3, and 6.3, respectively.

In the case of $(PbS)_{6.7}Y_{ITO}|Pt_{FTO}$, the IPCE spectrum (Figure 5c) shows that the wavelength at which the IPCE maximum appears (497 nm) nearly coincides with $\lambda_{max}$ of $(PbS)_{6.7}Y_{ITO}$ (495 nm). However, the IPCE spectrum of $(PbS)_{6.7}Y_{ITO}|Pt_{FTO}$ does not extend beyond 800 nm, at which the absorption of the interconnected QDs ends.[31] This result shows that in the case of $(PbS)_{6.7}Y_{ITO}|Pt_{FTO}$, the species that contribute to the photovoltaic effects are also interconnected QDs but not isolated and mesosized QDs. The IPCE value at the maximum IPCE wavelength (497 nm) was 2.2%. Thus, although the extinction coefficient is much higher than that of CdS, the photovoltaic efficiency of the interconnected PbS QDs is negligible compared to that of CdS QDs.

In the case of $(CdS)_{6.3}Y_{ITO}|(PbS)_{6.7}Y_{ITO}$, the IPCE spectrum (Figure 5d) matched very well with the absorption spectrum of


dx.doi.org/10.1021/la2025395 |*Langmuir* 2011, 27, 14678–14688

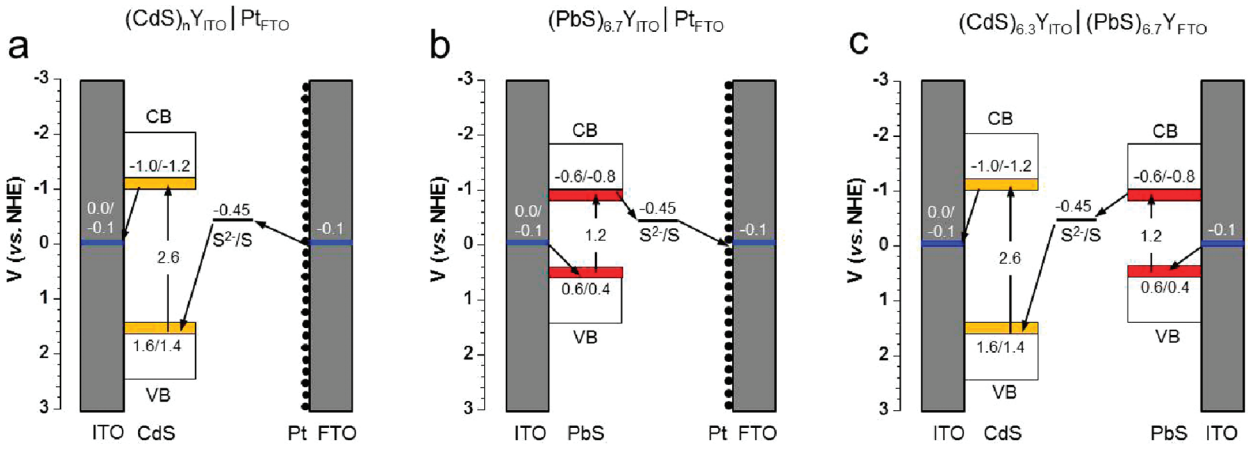


**Figure 4.** Schematic illustrations of the energy levels of the valence band and conduction band edges and the overall electron flow in the three solar cells (as indicated).

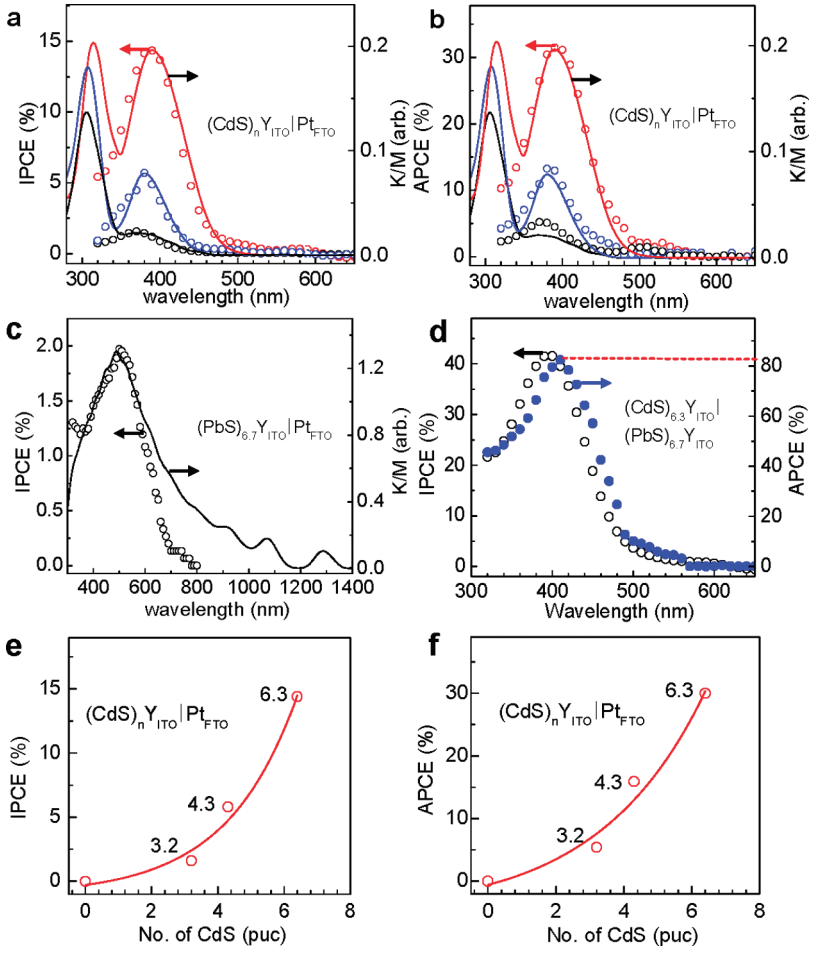


**Figure 5.** Overlay of IPCE and diffuse-reflectance spectra of $(CdS)_nY_{ITO}|Pt_{FTO}$ for $n$ = 3.2, 4.3, and 6.3 (a), APCE and diffuse reflectance spectra of $(CdS)_nY_{ITO}|Pt_{FTO}$ for $n$ = 3.2, 4.3, and 6.3 (b), IPCE and diffuse reflectance spectra of $(PbS)_{6.7}Y_{ITO}|Pt_{FTO}$ (c), IPCE and APCE spectra of $(CdS)_{6.3}Y_{ITO}|(PbS)_{6.7}Y_{ITO}$ (d), and plots of IPCE (e) and APCE (f) with respect to the number of CdS molecules per unit cell (puc) for $(CdS)_nY_{ITO}|Pt_{FTO}$.

$(CdS)_{6.3}Y_{ITO}$. The observed maximum IPCE value was 42% at 398 nm, which is very high despite the fact that the number of interconnected CdS QDs is very small. Knowing that the contribution of interconnected PbS QDs to the IPCE spectrum is negligible, the corresponding APCE spectrum can be obtained on the basis of the absorption spectrum of $(CdS)_{6.3}Y_{ITO}$. The result shows that the maximum APCE value is 81% at 405 nm.


dx.doi.org/10.1021/la2025395 |*Langmuir* 2011, 27, 14678–14688

**Predicted Effects of Higher Loading.** In the case of $(CdS)_nY_{ITO}|Pt_{FTO}$, the plots of IPCE versus $n$ (Figure 5e) and APCE versus $n$ (Figure 5f) showed that the IPCE and APCE values increase exponentially with increasing $n$, as expressed in eqs 4 and 5, respectively.

$$\text{IPCE} = 0.78 \exp\left(\frac{n}{2.14}\right) - 1.07 \quad (4)$$

$$\text{APCE} = 4.61 \exp\left(\frac{n}{3.13}\right) - 5.22 \quad (5)$$

This result is quite intriguing, and the extrapolations of the curves predict that in the case of $(CdS)_nY_{ITO}|Pt_{FTO}$ the IPCE and APCE values will become higher than 100% as $n$ becomes larger than ~10 (SI-9). In other words, the above results predict that the realization of one-photon multielectron injection will be possible by increasing $n$ to higher than 10. Unfortunately, we could not increase $n$ any further at this stage because the film undergoes crack formation at higher $n$. We are currently working on the development of methods to increase the loading of CdS in zeolite Y films supported on ITO glass.

**Estimated Sizes and Band Gaps of Interconnected CdS and PbS QDs.** We have proven that the interconnected QDs are responsible for the photovoltaic effects. In the case of $(CdS)_{6.3}Y_{ITO}$, the $\lambda_{max}$ of the interconnected QD appears at 390 nm. This allowed us to estimate the average size of the interconnected CdS QDs to be about 3 nm on the basis of the size−$\lambda_{max}$ relationship reported for CdS QDs.[38] Likewise, the estimated average size of interconnected PbS QDs is about 3.5 nm on the basis of the size−$\lambda_{max}$ relationship reported for PbS QDs.[39] If their sizes are indeed 3−3.5 nm, then they would be easily detected by a high-resolution TEM. However, we were not able to detect 3−3.5 nm CdS and PbS crystals from the zeolite Y films. This indicates that the shapes of the 3−3.5 nm CdS and PbS QDs in zeolite Y are not spherical but rather adopt the spider-web-like loosely interconnected shapes made by the random 3D interconnection of several CdS monomers and dimers with sizes of less than 1 nm at the supercage windows, with each monomer or dimer occupying a supercage. Regarding the monomers, Calzaferri and co-workers also provided strong evidence of the existence of monomeric PbS in zeolite Y supercages, whose electronic absorption maximum appears at around 380 nm.[35]

The average band gap energy of the interconnected CdS QD was measured to be 2.6 eV on the basis of the IPCE spectrum of $(CdS)_{6.7}Y_{ITO}|Pt_{FTO}$ (SI-10). Likewise, the measured average band gap energy of the interconnected PbS QD based on the IPCE spectrum of $(PbS)_{6.7}Y_{ITO}|Pt_{FTO}$ was 1.2 eV (SI-10). We believe that this is quite reasonable because only interconnected QDs show photovoltaic effects (Figure 5a) and IPCE spectra nearly coincide with the absorption spectra.

**Assignment of Energy Levels.** On the basis of the literature values[39−42] and with the experimentally measured band gap energy of the interconnected CdS QDs (2.6 eV), we assign the lower band edge values of CB to be between −1.0 and −1.1 eV and the upper band edge values of VB to be between 1.4 and 1.6 eV (Figure 4a). Likewise, we assign the lower band edge values of CB of the interconnected PbS to be between −0.6 and −0.8 eV and the upper band edge values of VB to be between 0.4 and 0.6 eV (Figure 4b). The Fermi energy levels of ITO and FTO are assigned to be 0.0 eV in accordance with the literature values.[41,42] This allows us to understand that in $(CdS)_{6.3}Y_{ITO}|Pt_{FTO}$ (Figure 4a) the electron transfer from $Pt_{FTO}$ to S is in fact an uphill electron transfer process. This seems to be the reason that the overall efficiency $\eta$ is not very high (0.1% in the case of $CdS_{6.3}Y_{ITO}|Pt_{FTO}$). This also explains why there is a 3-fold increase in overall efficiency $\eta$ (Table 2) when $CdS_{6.3}Y_{ITO}$ is coupled with $(PbS)_{6.7}Y_{ITO}$. Thus, PbS QDs are in fact pumping the electrons from the lower energy level (0.0 eV) to the higher energy level (−0.6/−0.8 eV), making the electron transfer from ITO to S a downhill process. Recently, in a QD-sensitized $TiO_2$ solar cell, a large increase in the overall efficiency $\eta$ was also observed by replacing the Pt electrode with PbS.[43]

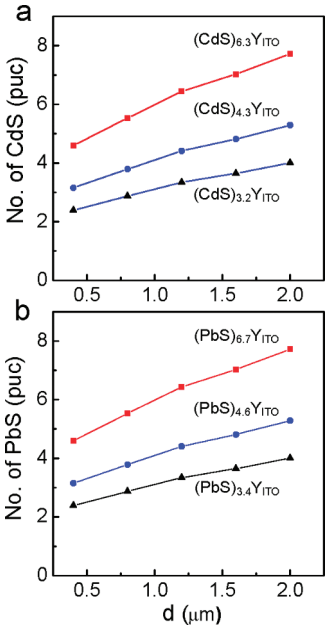


**Figure 6.** Plots of the number of CdS molecules in $(CdS)_nY_{ITO}$ (a) and PbS molecules in $(PbS)_nY_{ITO}$ (b) for each $n$ (as indicated) with respect to the depth of the zeolite Y film.

**Depth Profiles of QD Concentrations in Zeolite Y Films.** We measured the concentrations of CdS and PbS QDs on going from the external surfaces of $(CdS)_nY_{ITO}$ and $(PbS)_nY_{ITO}$, respectively, to the interiors (to the ITO sides) using a SEM equipped with energy-dispersive X-ray spectroscopy (EDS). The obtained depth profiles of $(CdS)_nY_{ITO}$ and $(PbS)_nY_{ITO}$ showed that the number of MCh QDs per unit cell, that is, the density of MCh QD, linearly decreased on going from the surface of $(CdS)_nY_{ITO}$ or $(PbS)_nY_{ITO}$ to the ITO glass (Figure 6).

**Intrazeolite Electron Transport between Interconnected QDs: Interdot Hoping versus Electrolyte-Mediated Interdot Electron Transport.** After understanding the overall electron flow pathways, the next question that arose was how the charge is transported from the QDs residing in the outermost layer to those placed inside and ultimately to those that are placed right next to the ITO electrode. We imagined two mechanisms, namely, electron hopping between the QDs (Figure 7a) and electrolyte-mediated charge transport (Figure 7b).

To study the feasibility of interdot electron hopping, we need to obtain an idea of the interdot distance to see whether interdot electron hopping is feasible at this distance. An independent calculation revealed that the total volume being occupied by CdS in $(CdS)_{6.3}Y_{ITO}$ is only 2.2%, which is a very small volume fraction (SI-11). On the basis of the average size of the interconnected CdS QDs (3 nm) and the above volume fraction

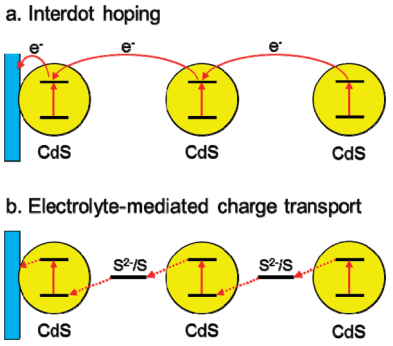


**Figure 7.** Schematic illustrations of the two intrazeolite charge transport mechanisms discussed in this work.

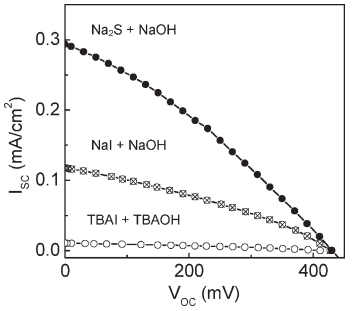


**Figure 8.** $I-V$ curves of $(CdS)_{6.3}Y_{ITO}|Pt_{FTO}$ with three different electrolytes (as indicated).

(2.2%), the estimated average edge-to-edge distance between the neighboring interconnected QDs was 5.6 nm (SI-12), which is about 7 times longer than the reported interdot distance (0.8 nm) of PbSe at which the carrier mobility becomes insignificant.[2]

In fact, the actual average interdot distance is likely to be much longer than 5.6 nm because of the fact that not all intrazeolite CdS is converted to the interconnected QDs. If 50% of the isolated QDs were converted to the interconnected QDs, then the average interdot distance becomes 8.2 nm, which is also plausible. Furthermore, the actual average interdot distance is likely to be even longer in the regions near the ITO glass because of the aforementioned phenomenon that the concentration of CdS decreases on going from the surface of the film to the ITO glass. Thus, the average edge-to-edge distance between the interconnected QDs in $(CdS)_{6.3}Y_{ITO}$ is remarkably large, even larger than the distance (~5 nm) at which the Coulombic energy transfer becomes negligible.

On the basis of the above, it is difficult to conceive that the electrons hop between the interconnected QDs, leading to overall charge transport from the QDs placed in the outermost layers of $(CdS)_nY_{ITO}$ or $(PbS)_{6.7}Y_{ITO}$ to the QDs placed next to the ITO glass. Indeed, we observed no photovoltaic effect from a dry cell made by depositing an Al-layer electrode onto $(CdS)_{6.3}Y_{ITO}$.

An alternative mechanism would be electrolyte-mediated charge transport from the outermost QDs to the QDs placed right next to the ITO glass. Calzaferri and co-workers also emphasized the importance of the electrolyte-mediated intrazeolite electron transfer.[44−46] To study this mechanism, we prepared two new cells having different electrolytes. The new electrolytes are the aqueous solution of NaI (0.1 M) and NaOH (1 M) and the aqueous solution of tetrabutylammonium iodide

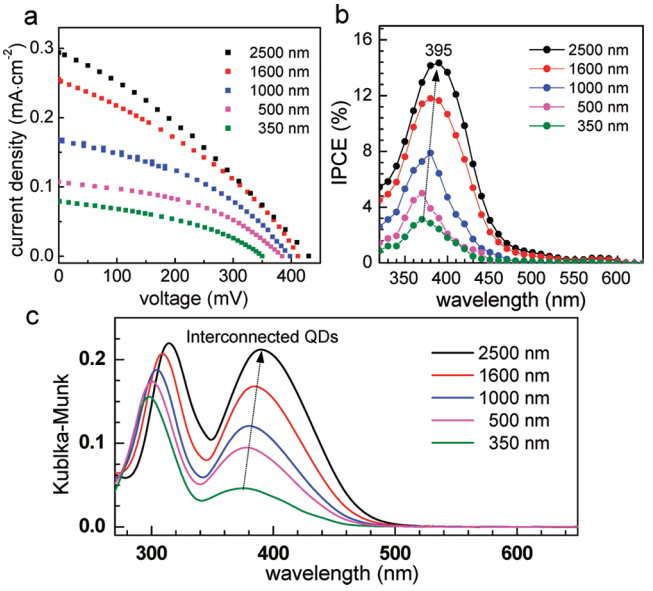


**Figure 9.** $I-V$ curves (a) and IPCE spectra (b) of $(CdS)_{6.3}Y_{ITO}|Pt_{FTO}$ with different thicknesses (as indicated).

(TBAI, 0.1 M) and tetrabutylammonium hydroxide (TBAOH, 1 M). In the case of the NaI and NaOH electrolyte solution, the photovoltaic effect was observed although the overall efficiency was lower than in the case where the standard electrolyte solution consisting of $Na_2S$ (0.1 M) and NaOH (1 M) was used (Figure 8). However, when the electrolyte solution consisting of TBAI and TBAOH was used, no photovoltaic effect was observed. Because $TBA^+$ cannot enter the zeolite Y cages, this result indicates that the inclusion of salts in the zeolite Y film is essential for the photovoltaic effect to appear. Indeed, the analyses of the zeolite Y film revealed that some electrolytes enter the zeolite Y films even after dipping the film in the electrolyte solution for 10 min, except when TBAI and TBAOH were used as the electrolytes (SI-13). On the basis of this, we conclude that the electrolyte-mediated charge transport (Figure 7b) operates inside zeolite Y films to complete the overall electron flow.

It is also important to check the possibility of whether the zeolite Y films have microcracks in which $Na_2S$ aggregate and set up percolation pathways for charge transport. For this purpose, we obtained confocal fluorescence microscopy images of the zeolite films that were stained with 2-(6-hydroxy-3-oxo-(3H)-xanthen-9-yl) benzoic acid (fluorescein) (SI-14). For comparison, we also prepared zeolite Y films that have microcracks. The comparison of the two fluorescein-stained zeolite Y films showed that the zeolite Y films that we have been using under our conditions are free from microcracks.

**Effect of Film Thickness.** Alternatively, one can argue that a very thin (~50−100 nm) QD layer that is intimately contacting the ITO glass is responsible for the photovoltaic action of $(CdS)_{6.3}Y_{ITO}$. In such a case, the $I-V$ curve should not be affected by the thickness of $(CdS)_{6.3}Y_{ITO}$ because the thickness of the thin, intimately contacting layer will remain constant regardless of the thickness as long as the film is thick enough (≳100 nm). To determine the validity of this alternative mechanism, we prepared $(CdS)_{6.3}Y_{ITO}$ in various thicknesses, namely, 350, 500, 1000, 1600, 2500 nm, and obtained their $I-V$ curves (Figure 9a). However, the $I_{sc}$, $V_{oc}$, and maximum IPCE


dx.doi.org/10.1021/la2025395 |*Langmuir* 2011, 27, 14678–14688

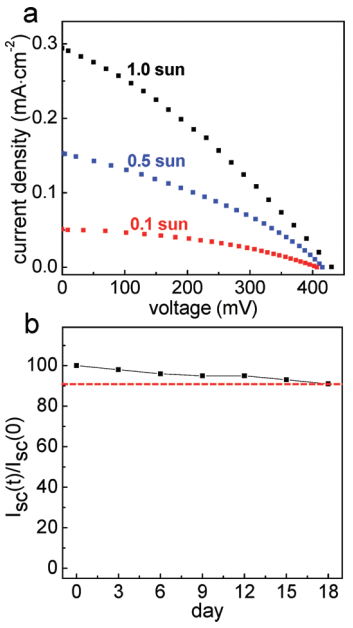


**Figure 10.** $I-V$ curves of $(CdS)_{6.3}Y_{ITO}|Pt_{FTO}$ under different light intensities (as indicated) (a) and plot of the short circuit current of $(CdS)_{6.3}Y_{ITO}|Pt_{FTO}$ at a certain time with respect to the initial value $[I_{sc}(t)/I_{sc}(0)]$ with time (b).

value progressively decreased as the thickness decreased, clearly showing that the photovoltaic effect strongly depends on the total number of CdS QDs.

Interestingly, the $\lambda_{max}$ at which IPCE gives the maximum value is red shifted from 370 to 395 nm with increasing thickness from 350 to 2500 nm (Figure 9b). Consistent with this, the absorption maximum of the interconnected CdS QDs progressively red shifted from 375 to 390 nm upon increasing the thickness from 350 to 2500 nm, indicating that the average size of the interconnected CdS QDs increases with increasing thickness, in other words, the volume of the zeolite host (Figure 9c). The performance data are tabulated in SI-15.

**Effect of Light Intensities and Long-Term Stability.** In the case of $(CdS)_nY_{ITO}|Pt_{FTO}$, upon increasing the loading ($n$), the short circuit current ($I_{sc}$) and open circuit voltage ($V_{oc}$) increased and the fill factor (FF) remains nearly constant. This gave rise to the increase in the overall efficiency ($\eta$). Thus, the efficiency of $(CdS)_{6.3}Y_{ITO}|Pt_{FTO}$ is 0.1% under the 1 sun condition. The efficiency increased by 30 and 50%, respectively, upon decreasing the light intensity to 0.5 and 0.1 sun, respectively (Figure 10a). The performance data under different light intensities are also tabulated in SI-16. Moreover, under the 1 sun condition, the efficiency of $(CdS)_{6.3}Y_{ITO}|Pt_{FTO}$ gradually decreased by only 10% even after irradiation of the cell for 18 days, indicating the remarkable stability of the intrazeolite QDs under the strongly illuminating conditions (1 sun) (Figure 10b).

In summary, we report for the first time the novel photovoltaic effects of CdS and PbS QDs encapsulated in zeolite Y films supported on ITO glass. The active species are interconnected QDs. CdS QDs are much more active than PbS QDs. $(CdS)_nY_{ITO}$ and $(PbS)_nY_{ITO}$ act as a photoanode and a photocathode, respectively, with Pt/FTO as the counter electrode. The reasons are not clear at this stage. However, this phenomenon indicates that the photoexcited electron residing in CB is readily injected into ITO glass in the case of CdS QDs but not in the case of PbS QDs. In the case of the latter, inefficient charge transfer to S occurs instead of charge injection into ITO glass. The photovoltaic efficiency of $(CdS)_nY_{ITO}$ increases by 3-fold upon employing $(PbS)_{6.7}Y_{ITO}$ as the counter electrode. When coupled with $(PbS)_{6.7}Y_{ITO}$, $(CdS)_{6.3}Y_f$ showed the maximum IPCE value (40%) and APCE value (81%) at 405 nm. This phenomenon is attributed to the pumping of electrons from ITO to S with the help of PbS QDs. The interdot charge transports mediated by occluded salt is responsible for the overall charge flow. In the case of $(CdS)_nY_{ITO}|Pt_{FTO}$, the one-photon multielectron generation phenomenon is predicted to take place at a loading level of higher than 10 CdS units per unit cell. This work thus reports the potential of QD-incorporating zeolite films to be developed into practically useful photovoltaic cells, giving a new direction to the application of zeolite-encapsulated QDs, and providing insight into the direction of the 3D QD array photovoltaic cells.

## ■ ASSOCIATED CONTENT

**Supporting Information.** Schematic illustration of the structure of the photovoltaic cells, photovoltaic characteristics under different light intensities, transmittance spectra of $(Na)_{59}Y_f$ and $(CdS)_nY_f$, effect of the thickness on the photovoltaic characteristics, effect of the sulfide source during the formation of CdS QD in zeolite Y on the photovoltaic performance, basis for the calculation of the volume percent of 6.3 CdS in a unit cell, calculation of the interdot distance between the interconnected CdS QDs in $(CdS)_{6.3}Y_f$, plots of IPCE and APCE with respect to the loaded number of CdS molecules per unit cell, and the extrapolation. This material is available free of charge via the Internet at http://pubs.acs.org.

## ■ AUTHOR INFORMATION

### Corresponding Author

*E-mail: yoonkb@sogang.ac.kr.

### Author Contributions

§These authors contributed equally.

## ■ ACKNOWLEDGMENT

This work was supported by the Korea Center for Artificial Photosynthesis located at Sogang University and funded by MEST through the National Research Foundation of Korea (NRF-2009-C1AAA001-2009-0093879) H.S.K. is grateful for Sogang University Research Grant 200910017

## ■ REFERENCES

(1) Luther, J. M.; Law, M.; Beard, M. C.; Song, Q.; Reese, M. O.; Ellingson, R. J.; Nozik, A. J. *Nano Lett.* **2008**, *8*, 3488–3492.

(2) Nozik, A. J.; Beard, M. C.; Luther, J. M.; Law, M.; Ellingson, R. J.; Johnson, J. C. *Chem. Rev.* **2011**, *110*, 6873–6890.

(3) Koleilat, G. I.; Levina, L.; Shukla, H.; Myrskog, S. H.; Hinds, S.; Pattantyus-Abraham, A. G.; Sargent, E. H. *ACS Nano* **2008**, *2*, 833–840.

(4) Johnston, K. W.; Pattantyus-Abraham, A. G.; Clifford, J. P.; Myrskog, S. H.; Hoogland, S.; Shukla, H.; Klem, J. D.; Levina, L.; Sargent, E. H. *Appl. Phys. Lett.* **2008**, *92*, 122111.

(5) Talapin, D. V.; Lee, J.-S.; Kovalenko, M. V.; Shevchenko, E. V. *Chem. Rev.* **2010**, *110*, 389–458.

(6) Debnath, R.; Tang, J.; Barkhouse, D. A.; Wang, X.; Pattantyus-Abraham, A. G.; Brzozowski, L.; Levina, L.; Sargent, E. H. *J. Am. Chem. Soc.* **2010**, *132*, 5952–5953.

(7) Choi, J. J.; Lim, Y.-F.; Santiago-Berrios, M. B.; Oh, M.; Hyun, B.-R.; Sun, L.; Bartnik, A. C.; Goedhart, A.; Malliaras, G. G.; Abruna, H. D.; Wise, F. W.; Hanrath, T. *Nano Lett.* **2009**, *9*, 3749–3755.
(8) Sambur, J. B.; Novet, T.; Parkinson, B. A. *Science* **2010**, *330*, 63–66.
(9) Kamat, P. V. *J. Phys. Chem. C* **2008**, *112*, 18737–18753.
(10) Mora-Seró, I.; Giménez, S.; Fabregat-Santiago, F.; Gómez, R.; Shen, Q.; Toyoda, T.; Bisquert, J. *Acc. Chem. Res.* **2009**, *42*, 1848–1857.
(11) Lee, H. J.; Yum, J.-H.; Leventis, H. C.; Zakeeruddin, S. M.; Haque, S. A.; Chen, P.; Seok, S. I.; Grätzel, M.; Nazeeruddin, M. K. *J. Phys. Chem. C* **2008**, *112*, 11600–11608.
(12) Leschkies, K. S.; Divakar, R.; Basu, J.; Enache-Pommer, E.; Boercker, J. E.; Carter, C. B.; Kortshagen, U. R.; Norris, D. J.; Aydil, E. S. *Nano Lett.* **2007**, *7*, 1793–1798.
(13) Yu, P.; Zhu, K.; Norman, A. G.; Ferrere, S.; Frank, A. J.; Nozik, A. J. *J. Phys. Chem. B* **2006**, *110*, 25451–25454.
(14) Buhbut, S.; Itzhakov, S.; Tauber, E.; Shalom, M.; Hod, I.; Geiger, T.; Garini, Y.; Oron, D.; Zaban, A. *ACS Nano* **2010**, *4*, 1293–1298.
(15) Baker, D. R.; Kamat, P. V. *Adv. Funct. Mater.* **2009**, *19*, 805–811.
(16) Huynh, W. U.; Dittmer, J. J.; Alivisatos, A. P. *Science* **2002**, *295*, 2425–2427.
(17) Liu, J.; Tanaka, T.; Sivula, K.; Alivisatos, A. P.; Fréchet., J. M. J. *J. Am. Chem. Soc.* **2004**, *126*, 6550–6551.
(18) Dayal, S.; Kopidakis, N.; Olson, D. C.; Ginley, D. S.; Rumbles, G. *Nano Lett.* **2010**, *10*, 239–242.
(19) Xi, D.; Zhang, H.; Furst, S.; Chen, B.; Pei, Q. *J. Phys. Chem. C* **2008**, *112*, 19765–19769.
(20) Breck, D. W. *Zeolite Molecular Sieves*; Wiley: New York, 1974.
(21) Herron, N.; Wang, Y; Eddy, M. M.; Stucky, G. D.; Cox, D. E.; Moller, K.; Bein, T. *J. Am. Chem. Soc.* **1989**, *111*, 530–540.
(22) Moller, K.; Eddy, M. M.; Stucky, G. D.; Herron, N.; Bein, T. *J. Am. Chem. Soc.* **1989**, *111*, 2564–2571.
(23) Stucky, G. D.; Mac Dougall, J. E. *Science* **1990**, *247*, 669–678.
(24) Liu, X.; Thomas, J. K. *Langmuir* **1989**, *5*, 58–66.
(25) Brigham, E. S.; Weisbecker, C. S.; Rudzinski, W. E.; Mallouk, T. E. *Chem. Mater.* **1996**, *8*, 2121–2127.
(26) Terasaki, O.; Yamazaki, K.; Thomas, J. M.; Ohsuna, T.; Watanabe, D.; Sanders, J. V.; Barry, J. C. *Nature* **1987**, *330*, 58–60.
(27) Ozin, G. A.; Steele, M. R.; Holmes, A. *J. Chem. Mater.* **1994**, *6*, 999–1010.
(28) Kim, J. J.; Kim, C. W.; Heo, N. H.; Lim, W. T.; Seff, K. *J. Phys. Chem. C* **2010**, *114*, 15741–15754.
(29) Sun, T.; Seff, K. *Chem. Rev.* **1994**, *94*, 857–870.
(30) Jeong, N. C.; Kim, H. S.; Yoon, K. B. *Langmuir* **2005**, *21*, 6038–6047.
(31) Kim, H. S.; Lee, M. H.; Jeong, N. C.; Lee, S. M.; Rhee, B. K.; Yoon, K. B. *J. Am. Chem. Soc.* **2006**, *128*, 15070–15071.
(32) Jeong, N. C.; Kim, H. S.; Yoon, K. B. *J. Phys. Chem. C* **2007**, *111*, 10298–10312.
(33) Kim, H. S.; Jeong, N. C; Yoon, K. B. *J. Am. Chem. Soc.* **2011**, *133*, 1642–1645.
(34) Brühwiler, D.; Seifert, R.; Calzaferri, G. *J. Phys. Chem. B* **1999**, *103*, 6397–6399.
(35) Leiggener, C.; Calzaferri, G. *Chem.—Eur. J.* **2005**, *11*, 7191–7198.
(36) Wong, K.-L.; Souici, A.; Waele, V. D.; Mostafavi, M.; Metzger, T. H.; Mintova, S. *Langmuir* **2010**, *26*, 4459–4464.
(37) Yordanov, I.; Knoerr, R.; Waele, V. D.; Mostafavi, M.; Bazin, P.; Thomas, S.; Rivallan, M.; Lakiss, L.; Metzger, T. H.; Mintova, S. *J. Phys. Chem. C* **2010**, *114*, 20974–20982.
(38) Yu, W. W.; Qu, L.; Guo, W.; Peng, X. *Chem. Mater.* **2003**, *15*, 2854–2860.
(39) Wang, C.; Thompson, R. L.; Ohodnicki, P.; Baltrus, J.; Matranga, C. *J. Mater. Chem.* **2011**, *21*, 13452.
(40) Bang, J. H.; Kamat, P. V. *ACS Nano* **2009**, *3*, 1467–1476.
(41) Park, Y.; Choong, V.; Gao, Y.; Hsieh, B. R.; Tang, C. W. *Appl. Phys. Lett.* **1996**, *68*, 2699–2701.
(42) Andersson, A.; Johansson, N.; Bröms, P.; Yu, N.; Lupo, D.; Salaneck, W. R. *Adv. Mater.* **1998**, *10*, 859–863.
(43) Tachan, Z.; Shalom, M.; Hod, I.; Rühle, S.; Tirosh, S.; Zaban, A. *J. Phys. Chem. C* **2011**, *115*, 6162–6166.
(44) Calzaferri, G.; Lanz, M.; Li, J.-W. *J. Chem. Soc., Chem. Commun.* **1995**, 1313–1314.
(45) Li, J.-W.; Pfanner, K.; Calzaferri, G. *J. Phys. Chem.* **1995**, *99*, 2119–2126.
(46) Li, J.-W.; Pfanner, K.; Calzaferri, G. *J. Phys. Chem.* **1995**, *99*, 12368–12369.